Bioactive Materials 6 (2021) 230–243

Contents lists available at ScienceDirect

Bioactive Materials

journal homepage: http://www.keaipublishing.com/biomat

Flexible electrical stimulation device with Chitosan-Vaseline® dressing accelerates wound healing in diabetes

Xiao-Feng Wang[a,1], Meng-Lu Li[b,1], Qing-Qing Fang[a], Wan-Yi Zhao[a], Dong Lou[a], Yan-Yan Hu[a], Jun Chen[c], Xiao-Zhi Wang[b,*], Wei-Qiang Tan[a,**]

[a] Department of Plastic Surgery, Sir Run Run Shaw Hospital, Zhejiang University School of Medicine, Hangzhou, 310016, Zhejiang Province, PR China
[b] Key Laboratory of Micro-Nano Electronic Devices and Smart Systems of Zhejiang Province, College of Information Science & Electronic Engineering, Zhejiang University, Hangzhou, 310027, Zhejiang Province, PR China
[c] Innovation Center for Signaling Network, College of Life Sciences, Zhejiang University, Hangzhou, 310058, Zhejiang Province, PR China

ARTICLE INFO

Keywords:
Diabetic wounds
Flexible electronic device
Electrical stimulation
Chitosan-vaseline® gauze
Wound healing

ABSTRACT

The healing process of diabetic wounds is typically disordered and prolonged and requires both angiogenesis and epithelialization. Disruptions of the endogenous electric fields (EFs) may lead to disordered cell migration. Electrical stimulation (ES) that mimics endogenous EFs is a promising method in treating diabetic wounds; however, a microenvironment that facilitates cell migration and a convenient means that can be used to apply ES are also required. Chitosan-Vaseline® gauze (CVG) has been identified to facilitate wound healing; it also promotes moisture retention and immune regulation and has antibacterial activity. For this study, we created a wound dressing using CVG together with a flexible ES device and further evaluated its potential as a treatment for diabetic wounds. We found that high voltage monophasic pulsed current (HVMPC) promoted healing of diabetic wounds *in vivo*. In studies carried out *in vitro*, we found that HVMPC promoted the proliferation and migration of human umbilical vein endothelial cells (HUVECs) by activating PI3K/Akt and ERK1/2 signaling. Overall, we determined that the flexible ES-chitosan dressing may promoted healing of diabetic wounds by accelerating angiogenesis, enhancing epithelialization, and inhibiting scar formation. These findings provide support for the ongoing development of this multidisciplinary product for the care and treatment of diabetic wounds.

1. Introduction

With the development of its economy and the new higher standards of living enjoyed by many of its citizens, China is now home to the largest population of individuals with diabetes worldwide [1]. Diabetic wounds, including diabetic foot ulcers, are identified as among the most severe complications of diabetes. Diabetic foot ulcers require long courses of treatment and remain highly susceptible to infections; these wounds have become a major cause of lower limb amputations not directly associated with external trauma [2]. The increased morbidity associated with diabetic wounds and the costs associated with long-term care of affected individuals have a significant negative economic impact on the healthcare economy in China [3]. Conventional treatments of diabetic wounds include debridement and frequent dressing changes; these modalities often do not result in a reliable or satisfactory outcome in terms of rapid wound closure [4–7]. As such, incremental improvements in diabetic wound care and treatment could result in significant benefits not only to patients but also to the country's entire healthcare economy.

In 1843, DuBois-Reymond reported his discovery of an electrical current at the site of a cut in one of his fingers [8]. Researchers called this phenomenon a “current of injury” and recognized that it resulted from the migration of charged cells participating in the process of wound healing. Intact skin has been determined to have an endogenous electrical potential and a transcutaneous current potential of 20–50 mV [9]. An injury to intact skin reduces the electric potential at the wound

Peer review under responsibility of KeAi Communications Co., Ltd.
* Corresponding author. Department of Plastic Surgery, Sir Run Run Shaw Hospital, Zhejiang University School of Medicine, 3 East Qingchun Road, Hangzhou, 310016, Zhejiang Province, PR China.
** Corresponding author. Key Laboratory of Micro-Nano Electronic Devices and Smart Systems of Zhejiang Province, College of Information Science & Electronic Engineering, Zhejiang University, No.38 Zheda Road, Hangzhou, 310027, Zhejiang Province, P.R.China.
E-mail addresses: xw224@zju.edu.cn (X.-Z. Wang), tanweixxxx@zju.edu.cn (W.-Q. Tan).
[1] These authors contributed equally to this work.

https://doi.org/10.1016/j.bioactmat.2020.08.003
Received 8 June 2020; Received in revised form 6 August 2020; Accepted 6 August 2020

compared to that detected in the surrounding intact skin area, thus generating a lateral endogenous electric fields (EFs) directed toward the center of the wound [10]; this EFs often plays a critical role in directing cell migration toward the wound [11,12]. The capacity of the endogenous EFs to promote cell migration is called “electrotaxis”; its properties include both directional vectors and activating mechanisms that stimulate charged cells involved in wound healing [13]. Electrical stimulation (ES) that mimics the potential to drive cell migration has been tested for decades; the results of numerous studies have led to the conclusion that ES might be utilized in improving wound healing [14–16]. When an external EFs is introduced, cells that participate in wound healing, including macrophages [17] and endothelial progenitor cells (EPCs) [18], move toward the cathode; by contrast, human dermal fibroblasts [19] move toward the anode.

The external microenvironment (i.e., regions immediately adjacent to wound surface) may have an indirect impact on the internal microenvironment (i.e., the cells and extracellular matrix adjacent to and beneath the surface of the wound) as part of a continuous exchange [20]. The external microenvironment is subject to changes in humidity, pH, and the presence or absence of microorganisms; these factors can have an immediate impact on the internal microenvironment of the wound via the expression of proinflammatory cytokines and matrix metallopeptidases (MMPs) that have an impact on cell migration and proliferation and therefore wound healing [21–23]. A wound microenvironment that retains moisture can promote and accelerate epithelial cell division and migration and can further improve the speed and quality of wound healing [24]. Likewise, bacterial contamination within a wound can alter its internal microenvironment via the expression of proinflammatory cytokines and MMPs; these factors have been identified to prevent healing as the wound becomes subject to a self-perpetuating inflammatory cycle [21]. Moreover, the extent and nature of bacterial colonization are also related to pH [25]. A chronic wound develops an alkaline pH, which then impairs healing by promoting invasive bacterial infection and contributes to the formation of biofilms [26]. Likewise, proteases secreted by the host or by the bacteria have higher activity at alkaline pH; this facilitates tissue proteolysis and the generation of toxic end-products [27].

Considering the importance of maintaining a healthy wound microenvironment, great progress has been made with respect to the design of wound dressings [28,29], providing a moist [30,31], antibacterial external microenvironment [32] and protecting the wound from environmental irritants [33]. Chitosan has been identified as an attractive biomaterial for wound care due to its antimicrobial characteristics and general biocompatibility [34–38]. Low molecular weight (MW) chitosan (< 100,000 Da) retains moisture, inhibits the growth of Gram-negative bacteria, and induces activation of complement. By contrast, high MW chitosan (> 100,000 Da) inhibits the growth of Gram-positive bacteria and regulates complement-mediated activities [39,40]. In our previous study, we have optimized the properties of chitosan by using a mixture of high MW and low MW forms [41]. However, chitosan solutions are viscous; dressings prepared with chitosan solution alone will adhere to the wound and promote tears in the granulation tissue during dressing changes that are not conducive to wound healing. By contrast, Vaseline gauze has been used for many years in a wide range of wound-healing applications; the presence of Vaseline® prevents wounds from sticking to the gauze and bacteria from contact with the skin [42]. The combination of chitosan and Vaseline® is designed to promote wound healing while retaining a moist microenvironment that limits bacterial contamination. Results from our previous study revealed that chitosan-Vaseline® gauze (CVG) is deemed more effective at promoting wound healing than Vaseline® gauze alone [43].

Endogenous EFs are likely to be damaged or absent in chronic wounds [44], which may result in limited activation and direction for cellular migration. ES can provide an exogenous EFs, thereby promoting cellular migration toward the wound bed. Likewise, CVG promotes moisture retention, immune regulation, and antibacterial effects and thus provides an appropriate microenvironment for wound healing. We hypothesize that ES and CVG may have complementary and synergistic effects with respect to the wound-healing process. However, ES devices in current use are large and not convenient for patient use. To address this issue, we explored the properties of polyimide (PI)-based devices; PI has been defined as a flexible material with biocompatibility, chemical stability, and heat resistance; this has been recently used to generate convenient and wearable medical devices [45]. As such, we manufactured a flexible ES-chitosan dressing that combines the advantages of a flexible ES device with the characterized wound-healing properties of CVG and explored its use as a therapeutic modality for the treatment of diabetic wounds.

We performed experiments both *in vivo* and *in vitro* aimed at optimizing the flexible ES-chitosan dressing. First, Sprague-Dawley (SD) rats were used to establish a model of type 2 diabetes mellitus (T2DM). Next, we used six electrical parameters based on pre-experimentation carried out *in vivo* together with literature searches [44,46–49]; two independent experiments were performed in order to optimize the electrical parameters; molecular mechanisms underlying the responses to optimized ES were then carried out *in vitro*. Subsequently, we used a flexible material (PI film) in order to manufacture an ES device using a flexible printing method; CVG was then added to generate the flexible ES-chitosan dressing. Finally, we verified the impact and the underlying molecular mechanisms using the flexible ES-chitosan dressing to promote wound healing *in vivo*.

2. Materials and methods

2.1. Manufacture of the flexible ES chitosan dressing

A total of 1.5 g of high MW (MW ~ 1,000,000 Da) and 1.5 g of low MW (MW ~5000 Da) chitosan (Golden-Shell Pharmaceutical Co., Zhejiang, China) was dissolved in a 1.0% glacial acetic acid solution (v/v) to generate a mixed chitosan solution (3%). Absorbent gauze was soaked in the mixed chitosan solution for 2 h to generate the chitosan gauze; this material was dried at 60–65 °C for 24 h to permit evaporation of the excess water. Vaseline® and paraffin oil were mixed in advance (2:1, w/w) and sterilized in a steam autoclave at 121 °C for 20 min. The dried chitosan gauze was then soaked in the Vaseline®-paraffin oil mix for 5 min. The ES device was manufactured using a flexible printing method based on the roll-to-roll process in the flexible printed circuit board factory using bendable PI as the substrate. Functional elements are integrated on the central part of the ES device, which were surrounded by flexible electrodes. Finally, the flexible ES device and CVG were fixed to one another by externally bonded spunlaced mesh-type cloth.

2.2. FTIR analysis and SEM

Fourier-transform infrared (FTIR) spectra were obtained on powders using a Bruker Tensor II Fourier-transform infrared spectrometer (BRUKER OPTICS, Ettlingen, Germany) at room temperature and ambient humidity with a spectral resolution of 4 cm^{-1} that were averaged over 32 scans. For scanning electron microscopy (SEM), samples were cut into small sizes, and each was coated with a thick layer of platinum. SEM images were taken using the Nova Nano SEM 450 scanning electron microscope (FEI, Brno, Czech Republic).

2.3. Animals

Specific pathogen-free male SD rats (4–6 weeks old, 100–120 g) were used in the study (Laboratory Animal Center of Zhejiang Academy of Medical Sciences, Hangzhou, China). All animal experiments were approved by the Zhejiang University Animal Care Committee. The experimental procedures and animal maintenance were performed in

accordance with the guidelines for animal experiments of the Institutional Animal Care and Use Committee of Zhejiang University.

2.4. T2D rat model establishment

All animals were fed a normal dry diet for 1 week during the acclimation period and then switched to a high fat and high glucose diet (Beijing Botai Hongda Biotechnology Co., Beijing, China). One month later, overnight-fasted animals were intraperitoneally injected with streptozotocin (STZ, Sigma-Aldrich, MO, USA) once with a dose of 35 mg/k [50,51]. Tail vein blood glucose was measured after 72 h and fasting blood glucose (FBG) ≥ 300 mg/dL was set as the evaluation criterion for successfully established T2D rat model [52,53]. Rats that did not satisfy the FBG criterion for two successive times after injection after the STZ injection were excluded from further study. Model rats were continuously fed with the high fat and high glucose diet in further studies.

2.5. Animal grouping

In this study, three independent animal experiments were performed. The first experiment was focused on the identification of optimal electrical parameters. A total of 36 rats with T2DM were randomly assigned into groups (6 rats/group) and evaluated as follows: group 1, high voltage monophasic pulsed current (HVMPC, 40V, 100 pulses per second (pps), 1% duty ratio); group 2, low voltage monophasic pulsed current (LVMPC, 4V, 100 pps, 1% duty ratio); group 3, direct current (DC, 4V); group 4, high voltage monophasic pulsed current plus direct current (HVMPC + DC, 40V, 100 pps, 1% duty ratio; 4 V); group 5, high voltage biphasic pulse current (HVBPC, 40V, 100 pps, 1% duty ratio); and group 6, low voltage biphasic pulse current (LVBPC, 4V, 100 pps, 1% duty ratio). Our preliminary experiments revealed that DC at 40V was too high as the rats were burned directly by the electrical current; as such, the high-voltage DC group was removed from subsequent evaluation. The pulsed current in the experimental groups was generated using an isolated pulse stimulator (A-M systems, USA); direct current was provided via a direct current power supply (Longwei, China). Two wounds (one on the left side and one on the right side of the body) were generated in each rat; the wounds on the right side were treated with ES and those on the left side were used as controls. A non-invasive approach designed to avoid electrical burns using a surface electrode was introduced for the second set of experiments. A total of 48 rats with T2DM were assigned randomly into one of the six groups described above; 30 rats (5 per group) were used to evaluate wound healing and another 18 rats (3 per group) were euthanized on day 7 after surgery for Western blot analysis. Conditions and methods were as described above, save for the use of a surface electrode in place of the insertion electrode. For the third experiment, 40 rats with T2DM (10 per group) were used to examine the impact of the flexible ES-chitosan dressing on wound healing. Three rats were euthanized on day 7 and day 15, and the wounds tissue include 5 mm unwounded skin were collected. Each of the two wounds generated in a single rat was treated identically. Groups for the third experiment include group 1, control; group 2, CVG alone; group 3, HVMPC alone; and group 4, flexible ES-chitosan dressing (HVMPC + CVG).

2.6. Wound healing study

All animals were anesthetized with isoflurane (2%) and the hair on their backs was removed using an electric shaver and depilatory cream (Weet, French). Two 2 × 2-cm^2 full-thickness skin sections (including the dartos), which were parallel to and**1** cm away from the midline, were excised on both sides of the dorsal skin. Then, wounds in experimental group was exposed to ES for 1 h once every 2 days, until the wound healed. Photographs of the wounds were taken. Surface areas of the wounds were measured and the relative wound areas were calculated using the Image J software (National Institutes of Health, USA). The healing rate of the wound was calculated according to the following formula:

$$\frac{\text{area of original wound-area of measured wound}}{\text{area of original wound}} \times 100\%$$

2.7. Histopathological examination

Samples were fixed overnight in 4% paraformaldehyde. Then, the tissues were dehydrated with graded series of ethanol and embedded in paraffin blocks. Tissue sections of 4 μm were stained with hematoxylin and eosin (H&E) to analyze re-epithelialization and scar tissue formation. The H&E slices were scanned at 10 × magnification with an Olympus VS120 Virtual Slide Microscope. The actual measurements of wound widths were calculated with the Image-Pro Premier 3D software (Media Cybernetics, MD, USA).

2.8. Immunohistochemistry

Briefly, deparaffinized sections were rehydrated using a graded ethanol series and then incubated with 3% H_2O_2 for 10 min. The slides were then washed thoroughly with PBS and blocked with 3% BSA at room temperature for 30 min. Sections were then incubated overnight at 4 ˚C with the primary antibodies. The primary antibodies used are listed in supporting information Table S1. The next day, the slides were incubated for 50 min at room temperature with HRP-conjugated goat anti-rabbit IgG secondary antibody (Servicebio, Wuhan, China). The staining was visualized after incubation with a DAB-H_2O_2 solution for 5 min and counterstaining with hematoxylin. Images were scanned at 10 × magnification with an Olympus VS120 Virtual Slide Microscope. The positive IOD/area in wound was calculated with the Image-Pro Premier 3D software.

2.9. Western blotting

Wound tissues were homogenized in the RIPA buffer mixed with a protease inhibitor cocktail (Thermo Scientific) by the KZ-II tissue lapping instrument (Servicebio, Wuhan, China). Human Umbilical Vein Endothelial Cells (HUVECs) suspended in the lysis buffer with the same components were vibrated for 30 s every 10 min. The homogenates were then centrifuged at 12,000 × *g* for 20 min at 4 ˚C and the supernatants were subsequently collected. Protein concentrations were determined using the Bradford assay kit (Bio-Rad, Hercules, CA, USA) and then diluted to 4 μg/μL. A total of 40 μg of protein were separated by the 4–12% gradient SDS-PAGE and transferred onto polyvinylidene membranes (Millipore, Bedford, MA, USA) at 250 mA for 90 min. After blocking with 5% nonfat milk at room temperature for 1 h, the membranes were incubated overnight at 4 ˚C with the primary antibody. The primary antibodies used are listed in supporting information Table S1. The next day, the membranes were incubated with a 1:5000 dilution of an HRP-conjugated anti-mouse or anti-rabbit secondary antibody (Proteintech, CHI, USA) at room temperature for 90 min. The membranes were then washed thoroughly with PBS three times and the immunoreactive bands were detected with an EZ-EL Kit (Biological Industries, Israel).

2.10. Cell culture and electrical stimulation in vitro

In order to examine the molecular mechanisms underlying the impact of monophasic pulsed current ES *in vitro*, the primary HUVECs (< 8 passages, ScienCell, CA, USA) were cultured in endothelial cell medium (ECM, ScienCell, CA, USA) with 5% fetal bovine serum, 1% endothelial cell growth supplement (ECGS, ScienCell, CA, USA), and 1% penicillin/streptomycin solution (P/S, ScienCell, CA, USA) at 37 ˚C

in a humidified atmosphere of 5% CO_2. The medium was changed every 2 days, and cells were passaged when cells reached 80% confluence. To mimic a high-glucose and high-fat environment, HUVECs were incubated in a medium supplemented with 25 mM D-glucose (Sigma-Aldrich, MO, USA) and 0.2–0.4 mM BSA-conjugated palmitate (Sigma-Aldrich, MO, USA) for 24h. HUVECs cultured in ECM medium containing 5.5 mM D-glucose, 19.5 mM L-glucose (Sigma-Aldrich, MO, USA), and 0.4 mM BSA were used as controls. For electrical stimulation, HUVECs in the experimental group were exposed to electrical stimulation environment using a C-Dish (Ion-Optics Co., MA, USA) and an isolated pulse stimulator (A-M systems, USA). The stimulating carbon electrodes were placed in the wells and submerged in the media.

2.11. Cell proliferation and apoptosis assays

Cell proliferation was analyzed using a Cell-Light 5-ethynyl-2′-deoxyuridine (EdU) Apollo567 In Vitro Kit (RiboBio, Shanghai, China) in strict accordance with the manufacturer's instructions. Images were acquired at 20 × magnification with a fluorescence microscope (Leica, Solms, Germany). EdU-positive cells were counted in the selected cells and calculated as the mean value from multiple fields of view. Cell apoptosis assays were performed using an Annexin V-PE 7-AAD Apoptosis Detection Kit (BD Biosciences, CA, USA) and terminal deoxynucleotidyl transferase-mediated dUTP-biotin nick end labeling assay (TUNEL assay, Beyotime, Shanghai, China) according to the manufacturer's protocol. For Annexin V-PE 7-AAD Apoptosis assay, the cells were analyzed the percentage of apoptotic cells, that cells undergoing early and late apoptosis, among 10,000–20,000 counted cells using a flow cytometer (BD Biosciences, CA, USA). For TUNEL assay, images of apoptosis cells were obtained using a microscope (Leica, Solms, Germany).

2.12. Cell migration assay

Cell migration testing was conducted using wound healing and Transwell assays. In order to obtain scratches of uniform length, a culture insert (ibidi, Munich, Germany) composed of two reservoirs was used in the wound healing assay. A cell suspension of 80 μL (3×10^4 cells/mL) was placed into each well and incubated in the CO2 incubator (37 °C, 5% CO2). After cell adherence, the insert was gently removed, creating a cell-free gap of 500 μm. Cells were thoroughly washed with PBS to remove the crossed cells. Every well was then filled with 2 mL of ECM medium containing 1% FBS and maintained in the incubator. At 0 and 24 h, images were taken using a fluorescence microscope (Leica, Solms, German). Transwell assay was performed according to the manufacturer's protocol. Briefly, 200 μL of the treated cells (2×10^5 cells) cultivated in serum-free DMEM were seeded into the upper chamber of the Transwell (Corning, NY, USA) with 8-μm pores and 500 μL of ECM medium containing 5% FBS were added to the lower chamber as a chemoattractant. After incubation for 24 h, the membrane was fixed in 4% paraformaldehyde and stained with 0.1% Crystal Violet (Solarbio, Beijing, China). The fixed cells in randomly selected fields were acquired at 20 × magnification using a microscope (Leica, Solms, German).

2.13. Statistical evaluation

Data were expressed as mean ± standard error of the mean (SE) and statistically analyzed by the GraphPad Prism 6.0 Software (GraphPad Software, CA, USA). The statistical difference significance between the stimulation groups and the control group was analyzed using the Student's *t*-test. Multiple group comparisons were analyzed by one-way ANOVA. *P*-values < 0.05 were considered statistically significant.

3. Results

3.1. Optimization of electrical parameters and electrodes to promote wound healing in diabetic rats

As wound healing progresses, the resistance of wound surface (primarily the epidermis) is seen to undergo a substantial increase [54]. An insertion electrode would have the capacity to apply voltage directly to the tissue without generating a current through the epidermis. However, using an insertion electrode in this series of experiments generated electrical burns in nearly all groups of rats. This complication was most apparent in the group subjected to DC, followed by those treated with high voltage (Supplementary Figs. 1a–c). However, the data revealed that administration of HVMPC resulted in accelerated wound closure (Supplementary Figs. 1d–h). When compared with the results from all other groups, rats treated with HVMPC underwent more rapid healing than did the control wounds (Supplementary Figs. 1i–k). As such, we concluded that HVMPC was the most effective electrical parameter among those evaluated although, as performed, it was associated with significant adverse events.

Then, we designed a separate animal experiment by using surface electrode; this modality has been currently the widely accepted ES therapy. Compared to the insertion electrode, surface electrode is non-invasive and easier to use; selection of electrical parameters for use with surface electrodes is more in-line with current clinical needs. Interestingly, similar results were obtained; HVMPC was selected as the better electrical parameter that might be used to accelerate wound healing. Our findings also revealed that administration of HVMPC significantly accelerated wound healing beginning on day 7 after surgery (Fig. 1) and did not result in electrical burns or any related adverse events.

Scar formation is an inevitable outcome after the injury of full-thickness skin; this process is characterized by the re-organization of the extracellular matrix (ECM) and the absence of normal skin appendages, such as hair follicles. H&E staining revealed that the healed wounds treated by stimulation with HVMPC were smaller than those of the control groups (Supplementary Fig. 2a). It also indicated that HVMPC has the better outcome of wound healing. Furthermore, wounds treated with HVMPC stimulation expressed higher levels of vascular endothelial growth factor (VEGF) compared to controls; this factor is deemed a critical activator of angiogenesis during wound healing (Supplementary Figs. 2b and c). Moreover, HVMPC stimulation resulted in an increase in the number of blood vessels at the wound sites compared to the controls (Supplementary Fig. 2d). Taken together, these data indicate that HVMPC may have accelerated wound healing in rats with T2DM via its capacity to promote angiogenesis.

3.2. Cell culture in high glucose/high palmitate to mimic the pathological environment associated with T2DM

We generated an *in vitro* model mimicking the microenvironment of wounds in patients with T2DM that included primary HUVECs cultured with high glucose (25 mM D-glucose) and a range of palmitate concentrations (0.2, 0.3, and 0.4 mM). TUNEL staining assay and Annexin V/7-AAD dual-color flow cytometry revealed that high glucose alone (25 mM D-glucose) in short-term culture had no impact on apoptosis of HUVECs when compared to cells in the control group (5.5 mM D-glucose, 19.5 mM L-glucose); by contrast, cellular apoptosis was observed in HUVEC cultures maintained in high levels of D-glucose with increasing concentrations of palmitate (0.2, 0.3, and 0.4 mM; Supplementary Figs. 3a–d). Wound healing and transwell assays have revealed that high levels of D-glucose alone had no impact on the migration of HUVECs; by contrast, diminished levels of HUVEC migration were observed in cultures that included a combination of high D-glucose and palmitate (Supplementary Figs. 3e–h). Likewise, proliferation of HUVECs was inhibited in the presence of both high D-glucose and

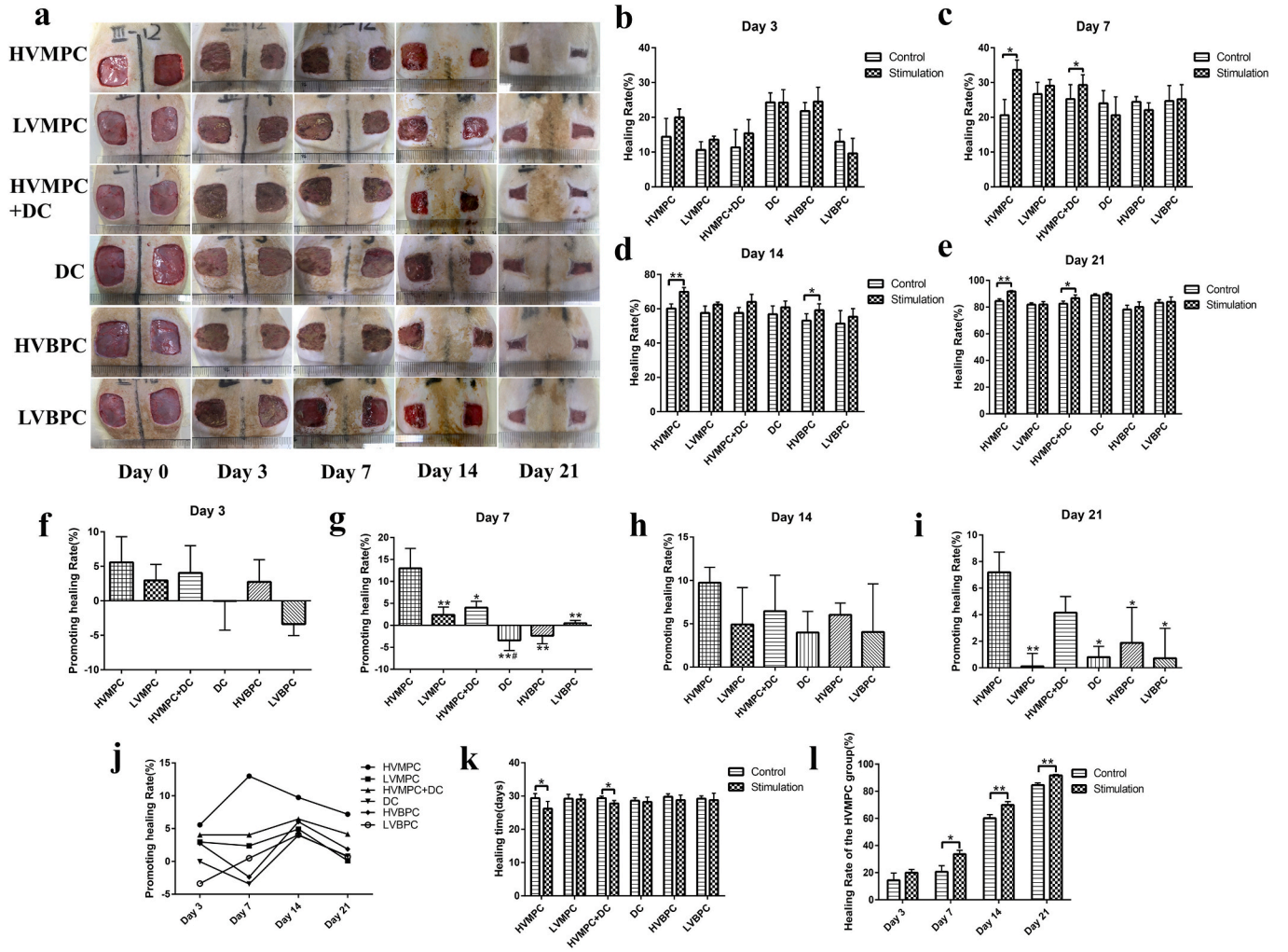

Fig. 1. High voltage monophasic pulsed current (HVMPC) was selected as the relatively optimal electrical parameter in T2DM rat wound model. (a) Photographs of the skin wounds placed on the rats in each of the 6 groups on days 0, 3, 7, 14, and 21 after surgery. (b–e) Statistical analysis comparing the rate of wound healing among rats in the 6 groups on days 3, 7, 14, and 21 after surgery. (f–i) Statistical analysis of the comparative rates of healing (healing rate of the ES-stimulated wound -healing rate of the control wound) in rats in each of the 6 groups on days 3, 7, 14, and 21 after surgery. (j) Trend chart denoting rates of wound healing among rats in each of the 6 groups. (k) Statistical analysis of healing time among rats in each of the 6 groups. (l) Statistical analysis of healing rate among rats in the HVMPC group. Groups evaluated include rats subjected to high voltage monophasic pulsed current (HVMPC), low voltage monophasic pulsed current (LVMPC), direct current (DC), high voltage monophasic pulsed current plus direct current (HVMPC + DC), high voltage biphasic pulse current (HVBPC), and low voltage biphasic pulse current (LVBPC). The left-side wound of each rat was used as the control, and the right-side wound was subjected to electrical stimulation. Data are presented as mean ± standard error of the mean (SE). Comparisons were performed using Student's t-test in (b–e), (k) and (l); $*P < 0.05$, $**P < 0.01$. Comparisons were performed using one-way analysis of variance (ANOVA) in (f–i); $*P < 0.05$, $**P < 0.01$ *vs.* the HVMPC group and $\#P < 0.05$ *vs.* the HVMPC + DC group.

palmitate; high levels of D-glucose alone had no impact on the HUVEC proliferation in short-term culture (Supplementary Figs. 3i and j).

3.3. HVMPC promoted the proliferation and migration capacity of HUVECs via activation of Akt and ERK1/2 signaling pathways

We performed experiments aimed at identifying the molecular mechanisms associated with HVMPC and its role in promoting angiogenesis. We detected a higher fraction of phosphorylated Akt (p-Akt) and phosphorylated extracellular signal-regulated kinase 1/2 (p-ERK1/2) in the cell cultures subjected to electrical stimulation compared to the controls (Supplementary Figs. 4a and 4b); no differences between the electrical stimulation groups were detected. Moreover, the results revealed that there were more proliferating HUVECs in the groups treated with HVMPC than were detected in the controls (Supplementary Figs. 4c and 4d). Moreover, as shown in Supplementary Figs. 4e and 4f, more cells were observed in the HVMPC group, which indicated the HVMPC group had faster cell migration.

In an effort to elucidate the mechanisms underlying ES using HVMPC and its role in promoting the proliferation and migration of HUVECs, the specific inhibitors of PI3K (LY294002) and ERK (U0126) were used to inhibit the activity of PI3K/Akt and ERK1/2 (Fig. 2a and b). HUVECs treated with either LY294002 or U0126 resulted in significant suppression of cell migration and proliferation (Fig. 2c–e). Furthermore, compared to the control group (i.e., no HVMPC, no inhibitors), more migrating cells was detected in the HVMPC group, and fewer were detected in any of the inhibitor groups (Fig. 2f). Moreover, EdU cell proliferation assay revealed that HVMPC promoted HUVECs proliferation (as determined by the number of EdU-positive cells); the impact of HVMPC was blunted in cultures treated with either LY294002 or U0126 (Fig. 2g). As such, we concluded that HVMPC may serve to promote proliferation and migration of HUVECs via activation of PI3K/Akt and ERK 1/2 signaling pathways.

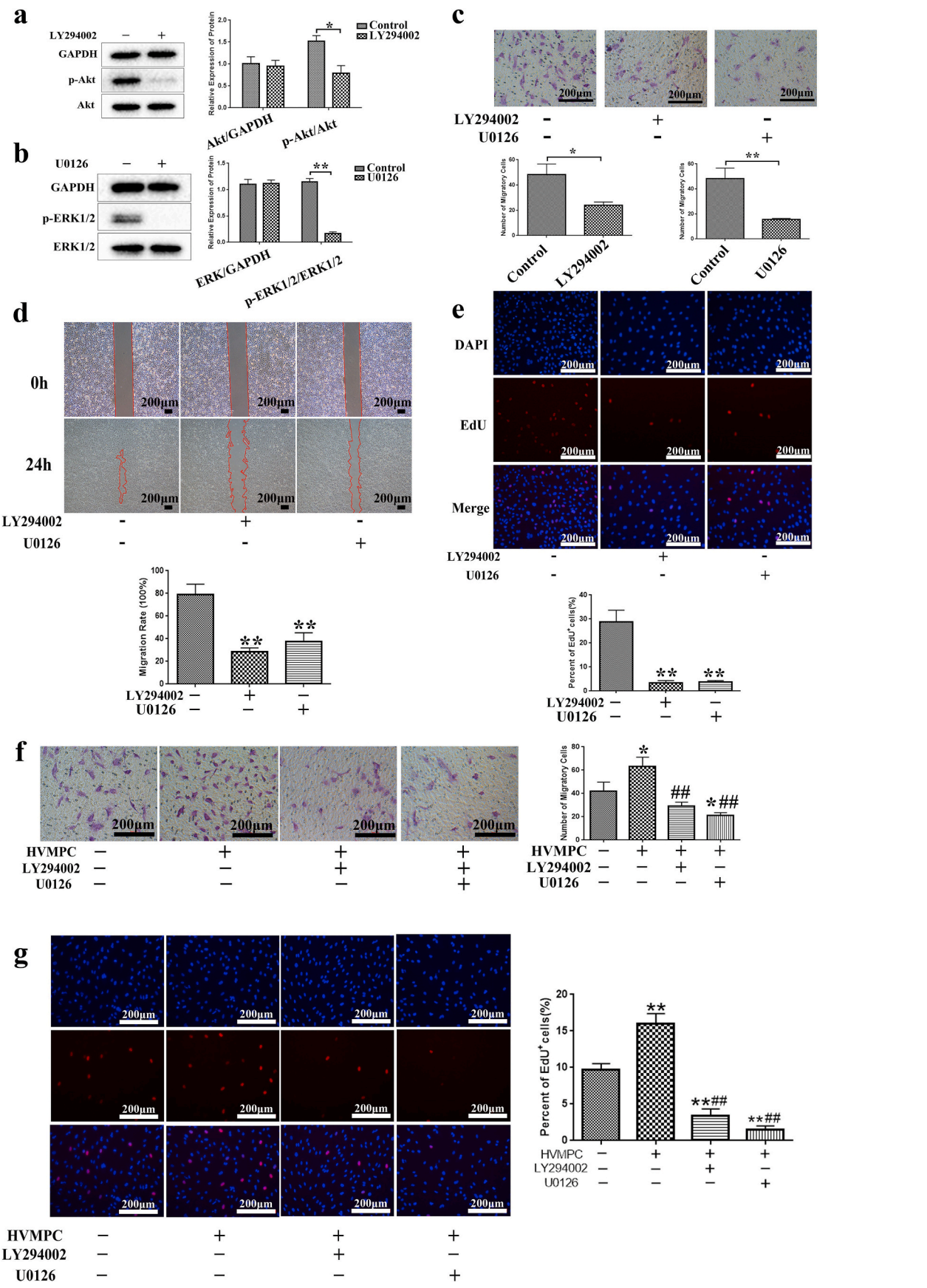

(caption on next page)

Fig. 2. HVMPC promoted proliferation and migration of HUVECs via activation of Akt and ERK1/2 signaling pathways. (a) The protein levels of Akt and p-Akt in HUVECs with and without addition of the inhibitor, LY294002 (b) The protein levels of ERK1/2 and p-ERK1/2 in HUVECs with and without addition of the inhibitor, U0126. (c) Images of transwell assays performed with HUVECs in the presence of LY294002 or U0126 (top) and quantitative analysis of migratory cells (below). (d) Images depicting the wound-healing assay (top) and statistical analysis of wound healing of HUVECs with the presence of LY294002 or U0126 (below). (e) Images of 5-ethynyl-2′-deoxyuridine (EdU) proliferation assays were acquired under a fluorescence microscope (20x, top) and quantitative analysis of proliferating (EdU^+) cells (below). (f) Images of transwell assay in HUVECs (left) and quantitative analysis of migratory cells (right). (g) Images from the EdU proliferation assay were acquired under a fluorescence microscope (20x, left) and quantitative analysis of proliferating (EdU +) cells (right). Data are presented as mean ± SE. Comparisons using Student's t-test were performed in (a), (b), and (c); *$P < 0.05$, **$P < 0.01$. Comparisons using one-way ANOVA were performed in (d–g); *$P < 0.05$, **$P < 0.01$ *vs.* control group, and ##$P < 0.01$ *vs.* HVMPC group.

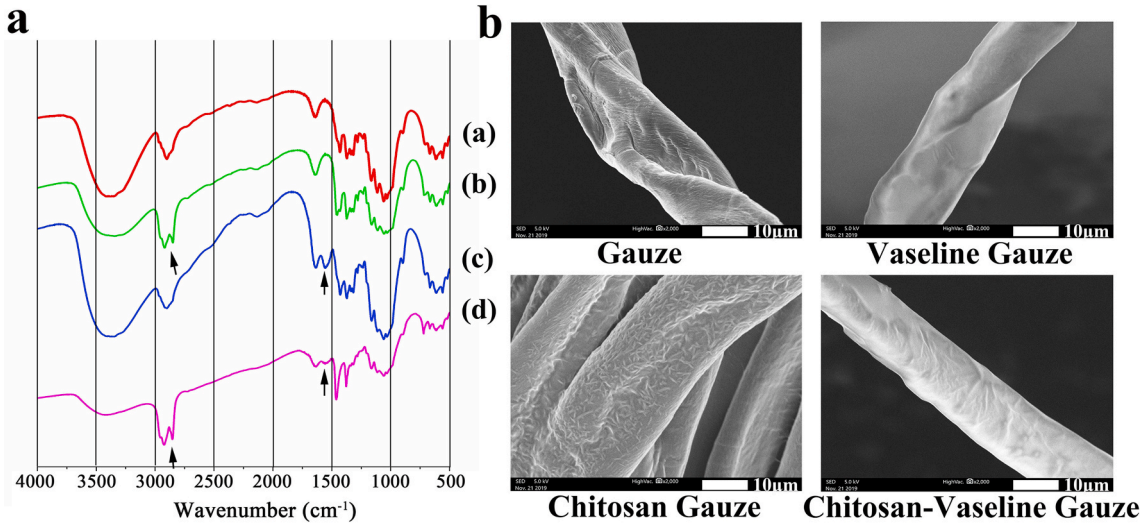

Fig. 3. Fabrication of a chitosan-Vaseline® gauze.. (a) The molecular structure of four different gauze preparations as determined by FTIR. (a) Gauze; (b) Vaseline gauze; (c) Chitosan gauze; (d) Chitosan-Vaseline® gauze; The peak at 1555 cm^{-1} was attributed to C═C stretching associated with chitosan; two peaks were detected (2800–3000 cm^{-1}) in samples that contained Vaseline®. (b) Scanning electron microscopy (SEM) images of the gauze surfaces.

3.4. Manufacture of the flexible-ES chitosan dressing

Based on aforementioned optimized results, we manufactured a flexible ES- chitosan dressing that consisted of a flexible ES device to be used together with CVG. CVG was generated by infiltration of gauze with both chitosan and Vaseline®. The result of FTIR spectroscopy of the chitosan-containing samples revealed a peak at 1555 cm^{-1}; this was attributed to C═C stretching. Two additional peaks (between 2800 and 3000 cm^{-1}) were detected in the samples that contained Vaseline®; these peaks were attributed to C–H stretching (Fig. 3a). The spectrum of CVG included both characteristic peaks; this finding indicates that both chitosan and Vaseline® were components of the final CVG formulation. SEM images of the surface of the gauze samples have been taken (Fig. 3b). These images revealed that chitosan adheres to the gauze fibers in a net shape; by contrast, fibers of the Vaseline®-embedded gauze are smooth and waxy. As anticipated, the gauze fibers of CVG are rougher than those of the Vaseline® gauze due to infiltration with chitosan.

The flexible ES device has included the same functional elements that are used to generate the rigid circuit board. The system diagram of the pulse generating circuit is presented in Supplementary Fig. 5a. The pulse modulation module is a microcontroller unit (MCU; STC12C2052AD) programmed in C to produce a pulse signal at P1.2 with a frequency of 100Hz, a duty cycle of 1%, and an amplitude of 5 V. The boost circuit includes a DC-to-DC converter control circuit chip (MC34063AP). The chip can be specifically designed to be incorporated in either step-down, step-up, or voltage-inverting applications (the voltage-inverting model can change the phase of voltage from positive to negative and vice versa). In this study, we built a step-up converter to generate a 30–40V DC output. The pin P1.2 of MCU and the output of MC34063AP are connected with the gate and drain of N-channel Metal Oxide Silicon Field Effect Transistor (MOSFET; FDN86501LZCN-D), respectively, in order to generate a pulse output with adjustable amplitude.

The schematic diagram is shown in Fig. 4a. The DC output of the step-up converter is controlled by R2 and R1 as per the following formula:

$$|V_{out}| = 1.25?1 + \frac{R_2}{R_1}?$$

According to the requirements of the study, the circuit should be capable of generating a pulse signal around 30–40V. Therefore, R1 and R2 were set at 10 kΩ and 390 kΩ, respectively, in order generate a 50V output. L2 and L7 were designed as a low-pass filters to reduce the ripple. In order to maintain flexible control of the output voltage, a variable resistor was set between the drain of the N-MOSFET and "boostout" pin. Because the maximum working current of the N-MOSFET at room temperature is 2.6A, and the maximum voltage required for this research application was 40V, the resistance value of the variable resistor should be no less than 15.3 Ω. The load will be connected parallel to the MOSFET. Therefore, when the output of the MCU is 0 V (gate-source voltage [VGS] < gate-source threshold voltage [VGS (th)]), the MOSFET will be closed, resulting in voltage applied on the load. By contrast, when the output of the MCU is 5 V (VGS > VGS [th]), the MOSFET will be opened, resulting in a short-circuited load.

The outputs of the MCU, the boost module, and the entire system were measured using a digital storage oscilloscope (SIGLENT SDS 2204X, Supplementary Figs. 5c–e). The actual output voltage of the boost module was restricted to 40 V due to the inductance of L2. By adjusting the variable resistance between the "boostout" pin and the "allout" pin, the voltage applied to the load can be adjusted from 0 to 40V to meet the application conditions.

After testing the performance of the rigid circuit board of the ES device (Fig. 4b and Supplementary Figs. 5b) and a flexible ES device

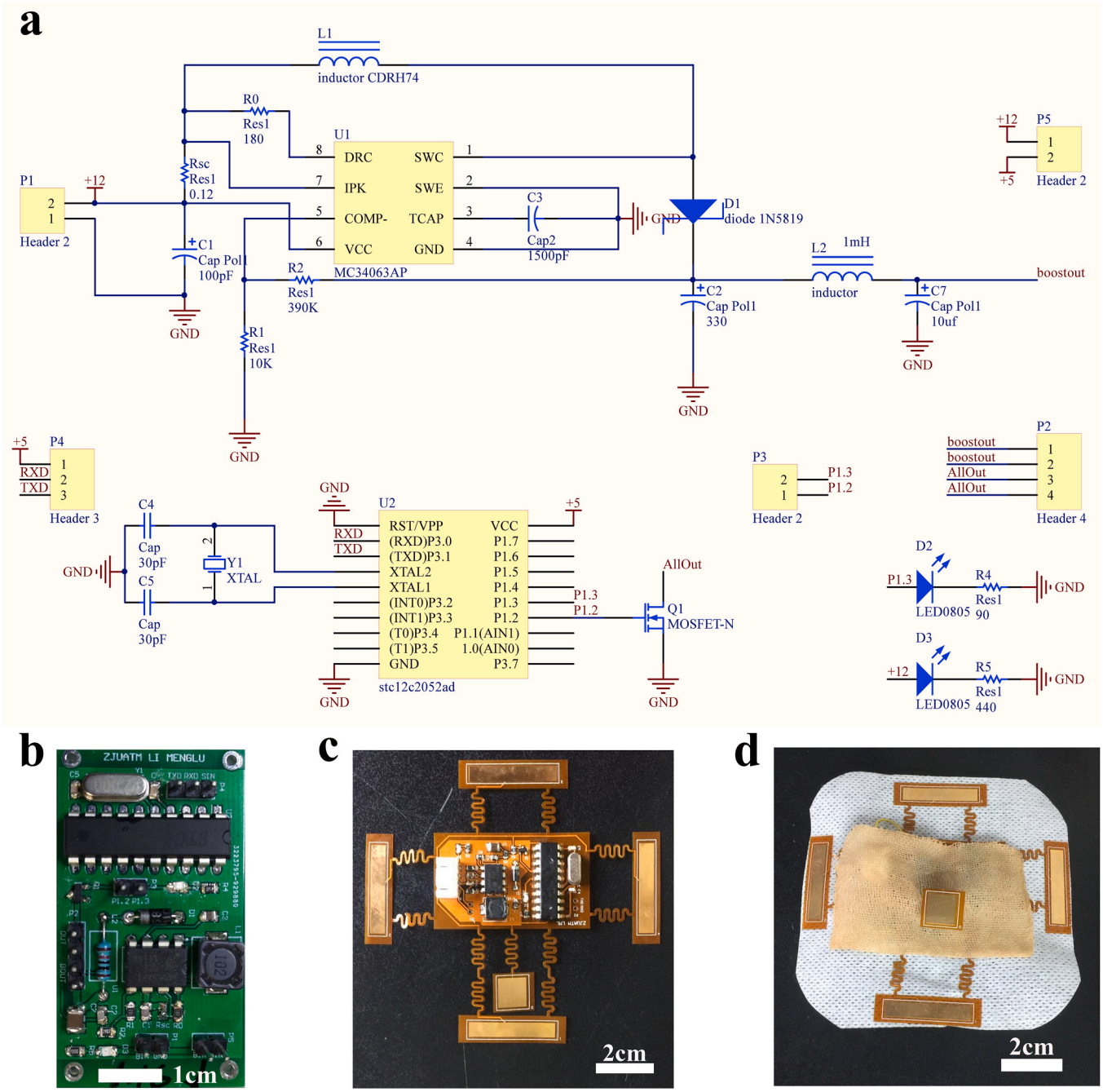

Fig. 4. Manufacture of a flexible ES-chitosan dressing. (a) Design diagram of the circuit board of the pulse generator that includes functional elements (e.g., DC-DC boost and pulse modulation modules). (b) The circuit board of the pulse generator. (c) The flexible ES device with flexible electrodes surrounded. (d) Flexible ES-chitosan dressing.

was manufactured that included the same functional elements. This was generated with a flexible printing method using PI film specially designed with a serpentine trace structure. The flexibility is enabled by the thin film geometry and the serpentine trace give the stretchable property (Fig. 4c). The serpentine trace structure includes two free-standing columns between each electrode and the central control element. The hierarchical degree of buckling associated with the serpentine trace structure ensures low levels of strain on the wires; this facilitates a reliable and stretchable connection [55] and permits the device to be applied to wounds that vary in size. Functional elements are integrated into the central part of the ES device and surrounded by flexible electrodes, including a DC-DC boost module and a pulse modulation module. Given the nature of the programmable element, the duty cycle and stimulus frequency could be adjusted *in situ* and in real time. Finally, the flexible ES device and CVG were fixed by externally bonded spun-laced mesh-type cloth(Fig. 4d).

3.5. Flexible-ES chitosan dressing promotes wound healing via upregulation of VEGF and activation of PI3K/Akt and ERK1/2 signaling pathways

Our findings revealed that the flexible ES-chitosan dressing accelerated wound healing as early as day 3 after surgery (Fig. 5a). Statistical analysis of the healing times and healing rates revealed that the flexible ES-chitosan dressing promoted accelerated wound healing compared to all other conditions evaluated (Fig. 5b and c). On day 7 after surgery, the results of Western blotting of wound tissue revealed

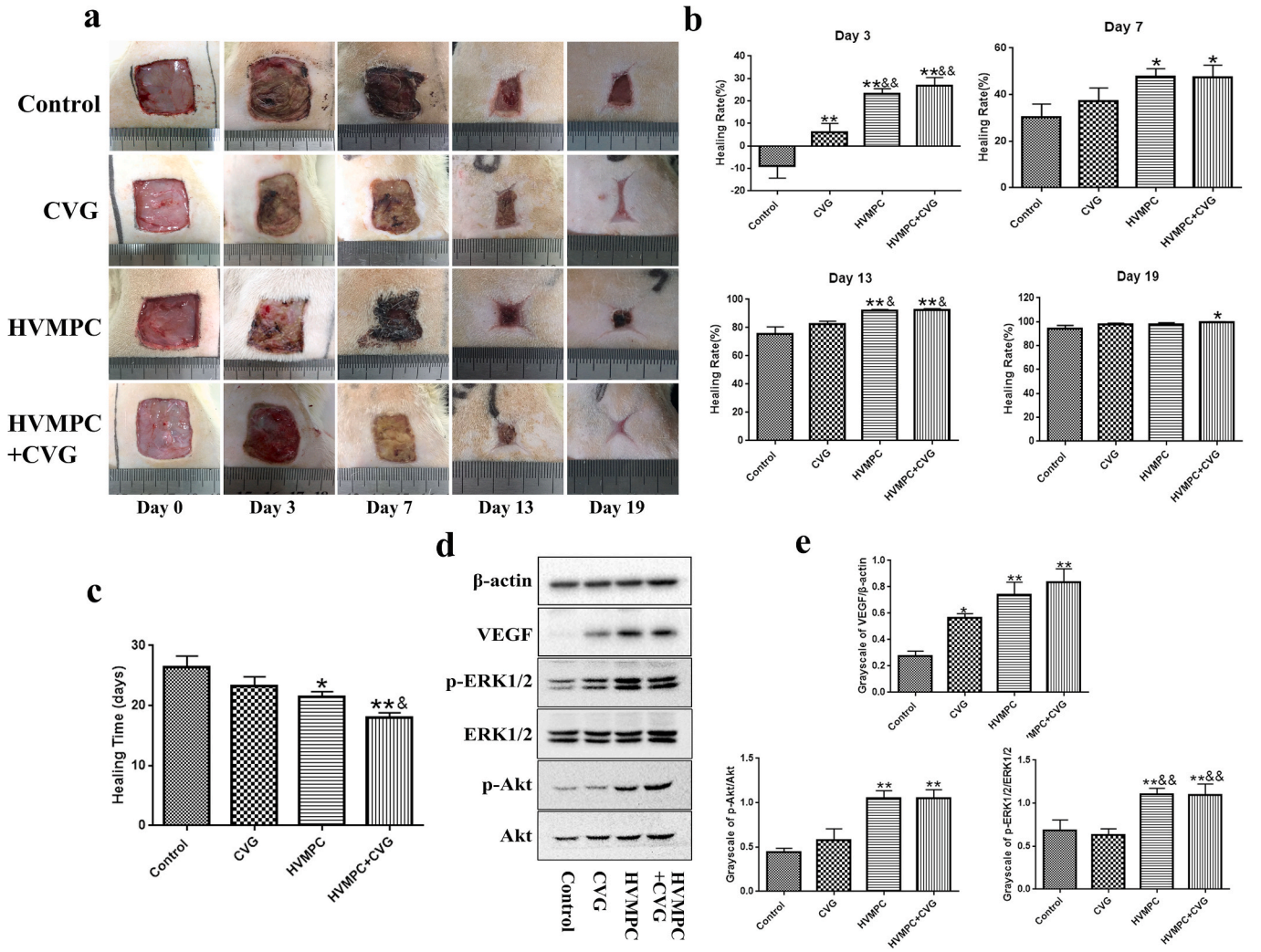

Fig. 5. Impact of flexible ES-chitosan dressing on wound healing. (a) Photographs of the skin wounds were taken from rats in each of the four groups on days 0, 3, 7, 13, and 19 after surgery. (b) Statistical evaluation of the rate of healing in the four groups on days 3, 7, 13, and 19 after surgery. (c) Statistical evaluation of healing time in the four groups. (d) Immunoreactive vascular endothelial growth factor (VEGF), Akt, p-Akt, ERK1/2, and p-ERK1/2 in the wound tissues of diabetes rats on day 7. Groups include the controls and those treated with CVG and with HVMPC and flexible ES-chitosan dressing (HVMPC + CVG). Data are presented as mean ± SE. Comparisons were performed using one-way ANOVA; $*P < 0.05$, $**P < 0.01$ *vs.* control group and $\&\&P < 0.01$ *vs.* CVG group.

that rats in groups that underwent treatment with HVMPC or CVG expressed higher levels of VEGF than did those in the control group; likewise, higher levels of p-Akt and p-ERK1/2 were detected in wound tissues from the rats treated with HVMPC (Fig. 5d and e). Moreover, immunohistochemical staining revealed increased expression of VEGF in all three experimental groups and higher levels of p-Akt and p-ERK1/2 in the two groups that underwent treatment with HVMPC (Supplementary Figs. 6a and 6b). These data suggest that the flexible ES-chitosan dressing promotes the expression of VEGF and activation of the PI3K/Akt and ERK1/2 pathways.

3.6. Flexible ES chitosan dressing accelerated wound epithelialization and inhibited scar formation

As shown in Fig. 6a, there was more epidermal tissue generated in the wounds of experimental groups compared to the controls. H&E staining revealed that the experimental group generated well-formed epidermal tissues compared to those observed among the controls at 15 days after surgery; at this time point, the epithelium of the group treated with flexible ES-chitosan dressings and HVMPC was nearly completely closed (Fig. 6b). Wound epithelialization may be accelerated under conditions in which the cells are presented with an appropriate microenvironment like what had happened in rats treated with CVG. In addition, after healing, the scars visible among rats treated with flexible ES-chitosan dressings were visibly smaller than those of the controls (Fig. 6c). Treatment with either CVG alone or with the flexible ES-chitosan dressing resulted in smaller scars; these results suggest that administration of CVG may suppress scar formation (Fig. 6d and e). Furthermore, results from H&E staining revealed that the widths of the healed wounds were also smaller among the rats treated with CVG compared to the control groups (Fig. 6f). Although only a few of the findings reached statistical significance, results from Western blotting have demonstrated a trend suggesting that either CVG or HVMPC may suppress phosphorylation of Smad 2 (p-Smad 2) and Smad 3 (p-Smad 3, Supplementary Fig. 7a). Similar trends were also found in immunohistochemical staining assays (Supplementary Figs. 7b–d).

4. Discussion

Chronic wounds are among the major complications of diabetes mellitus; these lesions tend to have a long-term negative impact on the patient's quality of life. Persistent hyperglycemia results in physiologic dysfunction at all stages of the wound-healing process largely attributed

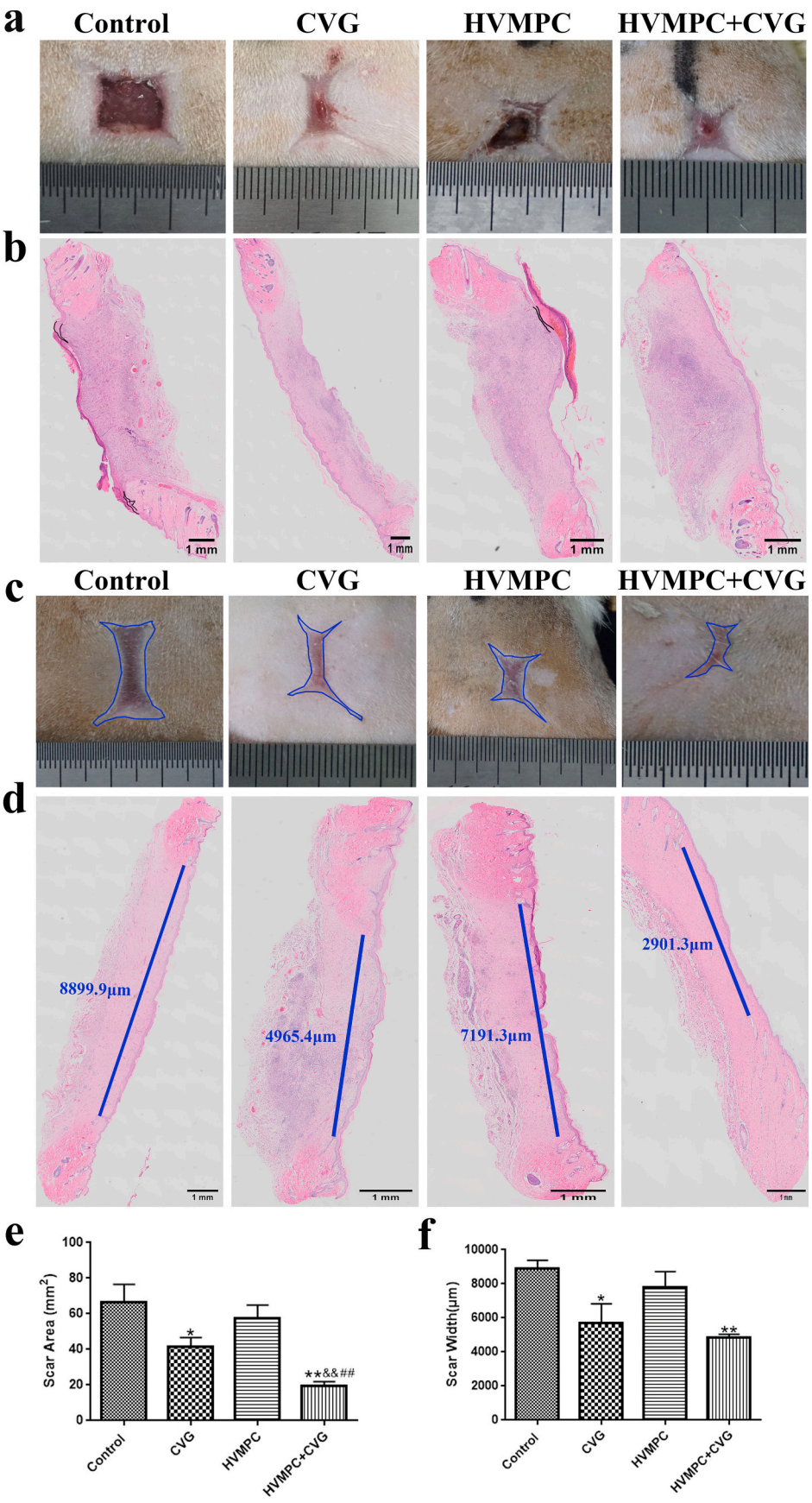

Fig. 6. Use of the flexible ES-chitosan dressing accelerated wound epithelialization and inhibited scar formation. (a) Image of a representative skin wound from post-surgical day 15. (b) Hematoxylin and eosin (H&E) stained sections of rat wound evaluated on day 15 after surgery. The black lines were used to demarcate regions of unhealed epidermis. Scale bar = 1 mm. (c) Representative image of wound scar evaluated on day 28 after surgery. The blue area represents the scar. (d) H&E stained sections of a wound evaluated on day 28 after surgery. The blue line represents the scar width. Scale bar = 1 mm. (e, f) Statistical evaluation of the scar area and width. Groups include control, CVG, HVMPC, and the flexible ES-chitosan dressing (HVMPC + CVG). Data are presented as mean ± SE. Comparisons were performed by ANOVA;*$P < 0.05$, **$P < 0.01$ *vs.* control group; &$P < 0.05$, &&$P < 0.01$ *vs.* CVG group; ##$P < 0.01$ *vs.* HVMPC group.

to the overproduction of reactive oxygen species. Likewise, it is widely appreciated that deranged angiogenesis, insufficient recruitment of circulating EPCs, and dysfunctional endothelial cells (ECs) migration and proliferation all serve to impair tissue repair in diabetic patients [56]. A full network of capillary blood vessels is critical for the delivery of oxygen, nutrients, and growth factors that are required for effective wound healing [57]. As such, methods that promote neovascularization and correct the hypoxic microenvironment are potentially effective for the treatment of diabetic wounds.

Wound healing has been determined to rely on the appropriate cellular migration, proliferation, differentiation, and secretory function. Cell migration toward the wound via chemotaxis and/or electrotaxis (in response to the endogenous EFs) is among the first steps in wound healing; these processes permit cells to be moved into position in order to facilitate their proliferation and differentiation [13]. As such, a rapid and orderly migration of cells into the wound is a critical first step in the wound-healing process. ES that mimics endogenous EFs is a promising method in treating diabetic wounds; however, a microenvironment that facilitates cell migration and a convenient means that can be used to apply ES are also required. In our previous study, CVG has been identified to facilitate wound healing; it also promotes moisture retention and immune regulation and has antibacterial activity. ES that mimics the endogenous EFs can promote cell migration toward the site of wound bed; likewise, CVG provides an appropriate microenvironment for cell migration and wound healing. As such, we hypothesized that the combination of ES and CVG might promote wound-healing process.

Previous studies have focused primarily on the impact of ES and their role in promoting wound healing (see Supplementary Tables 2 and 3). But no study has addressed whether a chitosan-based dressing with ES has the better effect on promotion the healing in diabetic wounds. Furthermore, there are numerous inconsistencies in the published literature with respect to electrical parameters, including electric current types; this has led to conflicting results and substantial uncertainty with respect to optimal electric current types (see Supplementary Tables 2 and 3). Moreover, ES device currently in clinical was large and not convenient to patients. Polyimide, flexible materials, have the advantage of flexibility, biocompatibility, and chemical stability. Thus, in the study, we manufactured a flexible ES-chitosan dressing that combined the advantages of a flexible ES device with the healing power of CVG. And, the dressing will be convenient for patient use.

In the first part of this manuscript, we compared the results of ES using six electrical parameters [44,46–49]. Our results indicated that HVMPC was the most effective means to promote diabetic wound healing; this finding is in agreement with the results from a previous meta-analysis [58]. One reason that high-voltage current may be superior to low-voltage current may relate to its capacity for greater depth of penetration [59]. Moreover, similar to the endogenous EFs, exogenous direct and monophasic pulsed current are both determined to exhibit polarity; by contrast, this is not a property of symmetric biphasic current (charge balanced), which does not mimic the physiological endogenous wound current [58] or promote electrotaxis, and is thus an undesirable selection for experiments of this nature. It is also critical to recognize that the duration of DC is always longer than 1 s; this results in irritating pH changes that are harmful to the skin and other tissues [60]. This may explain why DC was associated with the most serious electrical burns in this study. Thus, HVMPC has emerged as the relatively optimal parameter in generating an external EFs among the conditions evaluated here.

Moreover, we found that, when compared to controls, wounds treated with HVMPC expressed higher levels of VEGF, which is a well-known critical factor that promotes angiogenesis [61,62]; result in our speculation that HVMPC might promote wound healing by accelerating angiogenesis. Indeed, HVMPC resulted in an increased number of blood vessels at wound sites compared to what was observed in the control wound. As such, we explored the mechanisms underlying HVMPC on accelerating angiogenesis *in vitro*.

In order to reproduce conditions similar to those associated with T2DM *in vivo*, we examined senescence and apoptosis of HUVECs maintained in high-glucose and high-fat microenvironments *in vitro*. Previous studies have suggested that the combination of high concentrations of glucose and palmitate will simulate the pathologic microenvironment associated with poorly controlled T2DM [63,64] and will promote apoptosis of endothelial cells in a concentration-dependent manner [65]. In the study, short-term culture with concentrations of high D-glucose alone had no impact on apoptosis of HUVECs and likewise did not reduce their proliferative or migratory capacity; by contrast, the combination of high D-glucose with palmitate at 0.2, 0.3, or 0.4 mM has significantly increased HUVEC apoptosis as well as inhibited their proliferation and migration. Interestingly, there were no significant differences observed among the different palmitate concentrations; 0.2 mM palmitate was fully effective with respect to inducing cell senescence and apoptosis. Thus, in our subsequent experiments, these specific high-glucose (25 mM D-glucose) and high palmitate concentrations (0.2 mM) were used in an effort to mimic the high-glucose and high-fat microenvironment presented to the microvasculature in the setting of T2DM.

Mature ECs can proliferate and migrate to promote repair at sites of tissue damage [56]. Enhanced proliferative and migratory capacities of ECs will promote the ability to repair damaged blood vessels. In the study, we found that HVMPC promoted EC proliferation and migration more effectively than that observed among the controls. Moreover, we detected higher levels of p-Akt and p-ERK1/2 in groups treated with ES than among the controls. Previous studies revealed the PI3K/Akt and ERK1/2 pathways play critical roles with respect to cell proliferation and migration [66–68]; as such, we further hypothesized that signaling via the PI3K/Akt and ERK1/2 pathways might be involved in ES-mediated cell proliferation and migration. When these two pathways are blocked, HVMPC cannot promote cell proliferation and migration. From these findings, we concluded that HVMPC enhanced the proliferation and migration capacity of HUVECs via activation of PI3K/Akt and ERK1/2 signaling pathways.

With these optimized results, we manufactured a flexible ES-chitosan dressing that was effective toward promoting wound healing *in vivo*. Our results demonstrated that the use of flexible ES-chitosan dressing accelerated the wound-healing process. Our data also demonstrated that CVG and HVMPC both promote synthesis and secretion of VEGF, and HVMPC was associated with increased levels of p-Akt and p-ERK1/2. It is well established that VEGF is one of the most important angiogenic factors; it is produced primarily in macrophages [69]. VEGF promotes the growth of the blood vessels via its capacity to enhance the proliferative and migratory capacities of ECs [70]. Moreover, VEGF also affects the recruitment of EPCs to promote vasculogenesis and activates ECs to promote angiogenesis [71]. EPCs are mobilized by the actions of VEGF and are retained on the vascular surface by binding to adhesion molecules [72]. Once attached to the surface of injured ECs, EPCs undergo differentiation into ECs [56]. In addition to angiogenesis, activation of Akt and ERK phosphorylation also enhances the proliferative and migratory capacity of ECs in studies carried out *in vitro*. Normal vascularization includes the migration of EPCs to the sites of vascular damage and their differentiation into mature ECs; the mature ECs then undergo proliferation and migrate to sites at which repair of damaged cells is required.

Wound dressings are commonly used to manage wounds as they maintain a good wound microenvironment which plays an important role in wound healing processes [73]. It is necessary to emphasize that the factors of microenvironment, such as humidity, pH, and microorganisms, can impair the healing processes not only by their direct action on the wound microenvironment, but also because they are all related and can influence each other [74]. Bacterial contamination in a wound is believed to alter pH, and expression of proinflammatory cytokines and MMPs, keeping the wound stuck in a self-perpetuating

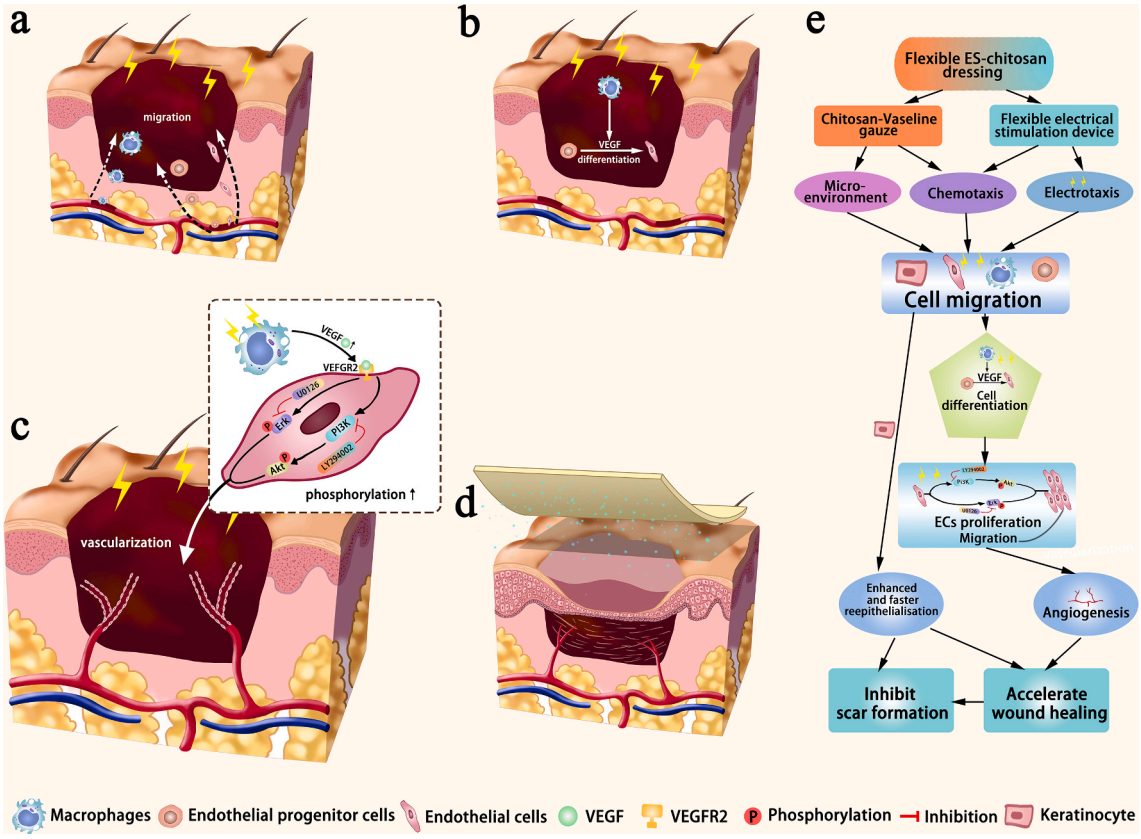

Fig. 7. Diagram depicting the healing mechanisms associated with the use of flexible ES-chitosan dressings. As shown, (a) macrophages, endothelial progenitor cells (EPCs), and endothelial cells (ECs) migrate to the sites of wound bed. (b) At this site, macrophages release VEGF, and EPCs undergo differentiation into mature ECs. (c) Administration of HVMPC enhances both proliferation and migration of mature ECs via activation of PI3K/Akt and ERK1/2 signaling pathways that promote repair of damaged vascular cells. (d) Finally, keratinocytes undergoing constant proliferation also migrate to the center of the wound.

inflammatory cycle [21,74]. The persistent inflammatory state, prolonging the presence of macrophages and neutrophils in the wound bed, which delays wound healing [21]. Moreover, the extent and nature of bacterial colonization are also related to pH [25]. A naturally occurring acidic environment represents a protective from bacteria. On the contrary, an alkaline microenvironment impairs wound healing by allowing bacterial infections and biofilm formation [26]. Changes in the microenvironment of wound, such as pH or bacterial infections, alter the balance the levels of proteases that plays a fundamental role in the wound healing phases [74,75]. In the study, in the process of making CVG, high MW and low MW chitosan was dissolved in a 1.0% glacial acetic acid solution, which providing acidic and antibacterial microenvironment that conducive to wound healing. In addition, it has been widely proved that a moist microenvironment increases the speed of epithelial cell migration and closure by superficial re-epithelialization [76]. A moist microenvironment is required so that the cells responsible for wound healing will be capable of functioning properly [77]. A moist wound microenvironment is beneficial to wound healing as it promotes rapid cell division and migration and further facilitates unimpeded movement of newly dividing epidermal cells into the wound [24,78]. In the study, we identified more well-formed epidermal tissues among the wounds treated with CVG and also among those treated with the flexible ES-chitosan dressings compared to the control group at 15 days after surgery. In this case, wound epithelialization may be accelerated due to the appropriate microenvironment provided by the CVG.

Scar formation is the physiological outcome of mammalian wound repair. A good wound healing process will reduce scar formation, and the disruption of the normal wound healing process, seem to be involved in excessive scarring [79]. Most chronic wounds fail to progress through the normal phases of wound repair, but remain in a chronic inflammatory state resulting from changing in the microenvironment of wound, such as pH or bacterial infections [80]. There is evidence that the amount of inflammation during the process of wound healing determines the extent of scar formation [81–83]. Moreover, wound secretions and cellular debris are seen to accumulate in dry wounds; these can impede cellular migration and form what is commonly known as a scab [78]. A well-maintained wound microenvironment leads to faster healing by preventing wound desiccation and the formation of scabs; scar formation is reduced in wounds maintained in moist as opposed to dry conditions [78,84]. Avoiding excess scabbing is advantageous not only for healing, but for positive cosmetic outcomes and more rapid restoration of the normal appearance of the skin [85]. In the study, after the wounds healed, smaller scars associated with the wounds that had been treated with flexible ES-chitosan dressing. And wounds that had undergone treatment with CVG alone also exhibited smaller scarred areas; these findings indicated that CVG may serve to suppress scar formation. Smaller scars may result from more rapid healing that occurs in response to the appropriate wound microenvironment provided by CVG.

Signaling via TGF-β/Smad has been considered as the main pathway involved in scar formation [86]. Sustained activation of the TGF-β/Smad signaling pathway results in long-term overactivation of fibroblasts and myofibroblasts which promotes excessive collagen formation in scars [87]. Smad2/3 are the main signaling molecules downstream of TGF-β; fibrosis secondary to Smad2/3 signaling has been demonstrated both *in vitro* and *in vivo* [88–90]. In the study, we detected a trend that suggested that the smaller scars associated with treatment using the flexible ES-chitosan dressing may be related to signaling via the Smad2/3 pathway. However, stronger evidence will be needed in order to define the specific mechanisms associated with the inhibition of scar

formation by the flexible ES-chitosan dressing.

Based on our results and proven mechanism in previous studies, we have provided a diagram that summarizes the potential mechanisms use by flexible ES-chitosan dressing to promote healing of diabetic wounds in Fig. 7. As what has been shown, HVMPC provides the impetus for cell migration which is facilitated by the appropriate local microenvironment provided by CVG. As such, macrophages, EPCs, and ECs migrate to the sites within the wound bed (Fig. 7a). HVMPC and CVG promote the release of VEGF by macrophages, which serves to mobilize EPCs which also migrate to this destination; these cells are retained on the vascular surface and undergo differentiation into mature ECs (Fig. 7b). HVMPC also promotes the proliferation and migration of mature ECs via activation of PI3K/Akt and ERK1/2; these cells are used to repair the damaged vasculature (Fig. 7c and Supplementary Fig. 8). During this period, the keratinocytes undergo constant proliferation and ultimately migrate to the center of the wound (Fig. 7d), resulting in its closure.

5. Conclusion

In this study, we have identified HVMPC as an effectively parameter that might be used in ES protocols for the treatment of diabetic wounds and we attempted to conduct an initial investigation of its underlying molecular mechanisms. In addition, we created a flexible ES-chitosan dressing that included a flexible ES device together with CVG; this modality promoted the healing of diabetic wounds by accelerating angiogenesis, enhancing epithelialization, and inhibiting scar formation. This dressing might be used in future clinical applications, particularly for the treatment of diabetic wound. In future studies, the dressing can incorporate sensors that will facilitate quantitative evaluation of wound conditions. Although animal models provide “value information”, it is also important to acknowledge the challenge to translate to humans and a considerable amount of research is needed.

CRediT authorship contribution statement

Xiao-Feng Wang: Conceptualization, Methodology, Investigation, Writing - original draft. **Meng-Lu Li:** Methodology, Investigation, Writing - original draft. **Qing-Qing Fang:** Methodology, Writing - original draft. **Wan-Yi Zhao:** Methodology, Investigation. **Dong Lou:** Writing - original draft. **Yan-Yan Hu:** Methodology. **Jun Chen:** Supervision. **Xiao-Zhi Wang:** Supervision, Writing - review & editing. **Wei-Qiang Tan:** Supervision, Writing - review & editing, Funding acquisition.

Declaration of competing interest

The authors declare no competing interests.

Acknowledgements

This work was supported by grants from National Natural Science Foundation of China (No. 81671918), National Key Research Program of China (2016YFC1101004) and Zhejiang Provincial Medical and Healthy Science Foundation of China (No. 2018KY874).

Appendix A. Supplementary data

Supplementary data to this article can be found online at https://doi.org/10.1016/j.bioactmat.2020.08.003.

References

[1] R.C.W. Ma, Epidemiology of diabetes and diabetic complications in China, Diabetologia 61 (2018) 1249–1260.
[2] Y. Zhu, Z. Cankova, M. Iwanaszko, S. Lichtor, M. Mrksich, G.A. Ameer, Potent laminin-inspired antioxidant regenerative dressing accelerates wound healing in diabetes, Proc. Natl. Acad. Sci. U. S. A. 115 (2018) 6816–6821.
[3] D. Huber, G. Tegl, A. Mensah, B. Beer, M. Baumann, N. Borth, C. Sygmund, R. Ludwig, G.M. Guebitz, A dual-enzyme hydrogen peroxide generation machinery in hydrogels supports antimicrobial wound treatment, ACS Appl. Mater. Interfaces 9 (2017) 15307–15316.
[4] N. Cullum, E.A. Nelson, K. Flemming, T. Sheldon, Systematic reviews of wound care management: (5) beds; (6) compression; (7) laser therapy, therapeutic ultrasound, electrotherapy and electromagnetic therapy, Health Technol. Assess. 5 (2001) 1–221.
[5] M. Konop, J. Czuwara, E. Klodzinska, A.K. Laskowska, U. Zielenkiewicz, I. Brzozowska, S.M. Nabavi, L. Rudnicka, Development of a novel keratin dressing which accelerates full-thickness skin wound healing in diabetic mice: in vitro and in vivo studies, J. Biomater. Appl. 33 (2018) 527–540.
[6] J.W. Chang, W. Heo, M.S.S. Choi, J.H. Lee, The appropriate management algorithm for diabetic foot: a single-center retrospective study over 12 years, Medicine (Baltim.) 97 (2018) e11454.
[7] A.F. Mavrogenis, P.D. Megaloikonomos, T. Antoniadou, V.G. Igoumenou, G.N. Panagopoulos, L. Dimopoulos, K.G. Moulakakis, G.S. Sfyroeras, A. Lazaris, Current concepts for the evaluation and management of diabetic foot ulcers, Efort Open Rev 3 (2018) 513–525.
[8] R. Nuccitelli, A role for endogenous electric fields in wound healing, Curr. Top. Dev. Biol. 58 (2003) 1–26.
[9] C. Martin-Granados, C.D. McCaig, Harnessing the electric spark of life to cure skin wounds, Adv. Wound Care 3 (2014) 127–138.
[10] A.T. Barker, L.F. Jaffe, J.W. Vanable Jr., The glabrous epidermis of cavies contains a powerful battery, Am. J. Physiol. 242 (1982) R358–R366.
[11] X. Li, J. Kolega, Effects of direct current electric fields on cell migration and actin filament distribution in bovine vascular endothelial cells, J. Vasc. Res. 39 (2002) 391–404.
[12] K.Y. Nishimura, R.R. Isseroff, R. Nuccitelli, Human keratinocytes migrate to the negative pole in direct current electric fields comparable to those measured in mammalian wounds, J. Cell Sci. 109 (1996) 199–207.
[13] M. Zhao, Electrical fields in wound healing-An overriding signal that directs cell migration, Semin. Cell Dev. Biol. 20 (2009) 674–682.
[14] L.C. Kloth, Electrical stimulation for wound healing: a review of evidence from in vitro studies, animal experiments, and clinical trials, Int. J. Low. Extrem. Wounds 4 (2005) 23–44.
[15] C. Lallyett, C.C. Yeung, R.H. Nielson, L.A.H. Zeef, D. Chapman-Jones, M. Kjaer, K.E. Kadler, Changes in S100 proteins identified in healthy skin following electrical stimulation: relevance for wound healing, Adv. Skin Wound Care 31 (2018) 322–327.
[16] H.K.R. Nair, Microcurrent as an adjunct therapy to accelerate chronic wound healing and reduce patient pain, J. Wound Care 27 (2018) 296–306.
[17] J.I. Hoare, A.M. Rajnicek, C.D. McCaig, R.N. Barker, H.M. Wilson, Electric fields are novel determinants of human macrophage functions, J. Leukoc. Biol. 99 (2016) 1141–1151.
[18] Z. Zhao, L. Qin, B. Reid, J. Pu, T. Hara, M. Zhao, Directing migration of endothelial progenitor cells with applied DC electric fields, Stem Cell Res. 8 (2012) 38–48.
[19] A. Guo, B. Song, B. Reid, Y. Gu, J.V. Forrester, C.A. Jahoda, M. Zhao, Effects of physiological electric fields on migration of human dermal fibroblasts, J. Invest. Dermatol. 130 (2010) 2320–2327.
[20] C.R. Kruse, K. Nuutila, C.C. Lee, E. Kiwanuka, M. Singh, E.J. Caterson, E. Eriksson, J.A. Sorensen, The external microenvironment of healing skin wounds, Wound Repair Regen. 23 (2015) 456–464.
[21] S.L. Percival, S. Finnegan, G. Donelli, C. Vuotto, S. Rimmer, B.A. Lipsky, Antiseptics for treating infected wounds: efficacy on biofilms and effect of pH, Crit. Rev. Microbiol. 42 (2016) 293–309.
[22] A. Lengheden, L. Jansson, Ph effects on experimental wound-healing of human fibroblasts in-vitro, Eur. J. Oral Sci. 103 (1995) 148–155.
[23] C.R. Kruse, M. Singh, S. Targosinski, I. Sinha, J.A. Sorensen, E. Eriksson, K. Nuutila, The effect of pH on cell viability, cell migration, cell proliferation, wound closure, and wound reepithelialization: in vitro and in vivo study, Wound Repair Regen. 25 (2017) 260–269.
[24] V. Falanga, Occlusive wound dressings. Why, when, which? Arch. Dermatol. 124 (1988) 872–877.
[25] H. Lambers, S. Piessens, A. Bloem, H. Pronk, P. Finkel, Natural skin surface pH is on average below 5, which is beneficial for its resident flora, Int. J. Cosmet. Sci. 28 (2006) 359–370.
[26] C.M. Stewart, M.B. Cole, J.D. Legan, L. Slade, M.H. Vandeven, D.W. Schaffner, Staphylococcus aureus growth boundaries: moving towards mechanistic predictive models based on solute-specific effects, Appl. Environ. Microbiol. 68 (2002) 1864–1871.
[27] N.B. Menke, K.R. Ward, T.M. Witten, D.G. Bonchev, R.F. Diegelmann, Impaired wound healing, Clin. Dermatol. 25 (2007) 19–25.
[28] G.D. Winter, Formation of the scab and the rate of epithelization of superficial wounds in the skin of the young domestic pig, Nature 193 (1962) 293–294.
[29] T.K. Hunt, Accelerated healing of full-thickness skin wounds in a wet environment - Discussion, Plast. Reconstr. Surg. 106 (2000) 613–614.
[30] B. Atiyeh, S. Hayek, An update on management of acute and chronic open wounds: the importance of moist environment in optimal wound healing, J Medicinal Chemistry Reviews 1 (2004) 111–121.
[31] M.G. Rippon, K. Ousey, K.F. Cutting, Wound healing and hyper-hydration: a counterintuitive model, J. Wound Care 25 (68) (2016) 70–75.
[32] F.L. Game, W.J. Jeffcoate, Dressing and diabetic foot ulcers: a current review of the evidence, Plast. Reconstr. Surg. 138 (2016) 158S–164S.

[33] G.D. Winter, Effect of air exposure and occlusion on experimental human skin wounds, Nature 200 (1963) 378–379.
[34] Y. Xie, Z.X. Yi, J.X. Wang, T.G. Hou, Q. Jiang, Carboxymethyl konjac glucomannan - crosslinked chitosan sponges for wound dressing, Int. J. Biol. Macromol. 112 (2018) 1225–1233.
[35] S. Yang, Y. Yang, S. Cui, Z. Feng, Y. Du, Z. Song, Y. Tong, L. Yang, Z. Wang, H. Zeng, Q. Zou, H. Sun, Chitosan-polyvinyl alcohol nanoscale liquid film-forming system facilitates MRSA-infected wound healing by enhancing antibacterial and anti-biofilm properties, Int. J. Nanomed. 13 (2018) 4987–5002.
[36] S. Ahmad, M.U. Minhas, M. Ahmad, M. Sohail, O. Abdullah, S.F. Badshah, Preparation and evaluation of skin wound healing chitosan-based hydrogel membranes, AAPS PharmSciTech 19 (2018) 3199–3209.
[37] H.K.R. Nair, Nano-colloidal silver and chitosan bioactive wound dressings in managing diabetic foot ulcers: case series, J. Wound Care 27 (2018) S32–S36.
[38] Q. Li, F. Lu, G. Zhou, K. Yu, B. Lu, Y. Xiao, F. Dai, D. Wu, G. Lan, Silver inlaid with gold nanoparticle/chitosan wound dressing enhances antibacterial activity and porosity, and promotes wound healing, Biomacromolecules 18 (2017) 3766–3775.
[39] I. Younes, M. Rinaudo, Chitin and chitosan preparation from marine sources. Structure, properties and applications, Mar. Drugs 13 (2015) 1133–1174.
[40] I. Younes, S. Sellimi, M. Rinaudo, K. Jellouli, M. Nasri, Influence of acetylation degree and molecular weight of homogeneous chitosans on antibacterial and antifungal activities, Int. J. Food Microbiol. 185 (2014) 57–63.
[41] W.Y. Zhao, Q.Q. Fang, X.F. Wang, X.W. Wang, T. Zhang, B.H. Shi, B. Zheng, D.D. Zhang, Y.Y. Hu, L. Ma, W.Q. Tan, Chitosan-calcium alginate dressing promotes wound healing: a preliminary study, Wound Repair Regen. 28 (2020) 326–337.
[42] C.S. Pak, D.H. Park, T.S. Oh, W.J. Lee, Y.J. Jun, K.A. Lee, K.S. Oh, K.H. Kwak, J.W. Rhie, Comparison of the efficacy and safety of povidone-iodine foam dressing (Betafoam), hydrocellular foam dressing (Allevyn), and petrolatum gauze for split-thickness skin graft donor site dressing, Int. Wound J. 16 (2019) 379–386.
[43] Q.Q. Fang, X.F. Wang, W.Y. Zhao, B.H. Shi, D. Lou, C.Y. Chen, M.X. Zhang, X. Wang, L. Ma, W.Q. Tan, Development of a chitosan-vaseline gauze dressing with wound-healing properties in murine models, Am. J. Trop. Med. Hyg. 102 (2020) 468–475.
[44] L.C. Kloth, Electrical stimulation technologies for wound healing, Adv. Wound Care 3 (2014) 81–90.
[45] B.C. Kim, J.Y. Hong, G.G. Wallace, H.S. Park, Recent progress in flexible electrochemical capacitors: electrode materials, device configuration, and functions, Adv Energy Mater 5 (2015).
[46] R.L. Kwan, G.L. Cheing, S.K. Vong, S.K. Lo, Electrophysical therapy for managing diabetic foot ulcers: a systematic review, Int. Wound J. 10 (2013) 121–131.
[47] M. Ashrafi, T. Alonso-Rasgado, M. Baguneid, A. Bayat, The efficacy of electrical stimulation in experimentally induced cutaneous wounds in animals, Vet. Dermatol. 27 (2016) 235-e57.
[48] A. Polak, A. Franek, J. Taradaj, High-voltage pulsed current electrical stimulation in wound treatment, Adv. Wound Care 3 (2014) 104–117.
[49] L.C. Kloth, Wound healing with conductive electrical stimulation—it's the dosage that counts, J Wound Technol 6 (2009) 30–37.
[50] W. Xu, J. Liu, D. Ma, G. Yuan, Y. Lu, Y. Yang, Capsaicin reduces Alzheimer-associated tau changes in the hippocampus of type 2 diabetes rats, PloS One 12 (2017) e0172477.
[51] M.M. Soliman, M. Abdo Nassan, T.A. Ismail, Origanum majoranum extract modulates gene expression, hepatic and renal changes in a rat model of type 2 diabetes, Iran. J. Pharm. Res. (IJPR) 15 (2016) 45–54.
[52] M.J. Oza, Y.A. Kulkarni, Formononetin treatment in type 2 diabetic rats reduces insulin resistance and hyperglycemia, Front. Pharmacol. 9 (2018) 739.
[53] N.C. Qiu, W. Li, M.E. Liu, X.X. Cen, C.X. Shan, W. Zhang, Q. Liu, Y. Wang, Y.T. Zhu, M. Qiu, Comparison of great curvature plication with duodenal-jejunal bypass (GCP-DJB) and sleeve gastrectomy (SG) on metabolic indices and gut hormones in type 2 diabetes mellitus rats, Obes. Surg. 28 (2018) 4014–4021.
[54] D.W. Spence, B. Pomeranz, Surgical wound healing monitored repeatedly in vivo using electrical resistance of the epidermis, Physiol. Meas. 17 (1996) 57–69.
[55] K. Krieger, Extreme mechanics: buckling down, Nature 488 (2012) 146–147.
[56] D. Rana, A. Kumar, S. Sharma, Endothelial progenitor cells as molecular targets in vascular senescence and repair, Curr. Stem Cell Res. Ther. 13 (2018) 438–446.
[57] H. Chen, P. Jia, H. Kang, H. Zhang, Y. Liu, P. Yang, Y. Yan, G. Zuo, L. Guo, M. Jiang, J. Qi, Y. Liu, W. Cui, H.A. Santos, L. Deng, Upregulating hif-1alpha by hydrogel nanofibrous scaffolds for rapidly recruiting angiogenesis relative cells in diabetic wound, Adv Healthc Mater 5 (2016) 907–918.
[58] C. Khouri, S. Kotzki, M. Roustit, S. Blaise, F. Gueyffier, J.L. Cracowski, Hierarchical evaluation of electrical stimulation protocols for chronic wound healing: an effect size meta-analysis, Wound Repair Regen. 25 (2017) 883–891.
[59] A. Scheiner, J.T. Mortimer, U. Roessmann, Imbalanced biphasic electrical stimulation: muscle tissue damage, Ann. Biomed. Eng. 18 (1990) 407–425.
[60] R.A. Newton, T.C. Karselis, Skin pH following high voltage pulsed galvanic stimulation, Phys. Ther. 63 (1983) 1593–1596.
[61] P. Losi, E. Briganti, C. Errico, A. Lisella, E. Sanguinetti, F. Chiellini, G. Soldani, Fibrin-based scaffold incorporating VEGF- and bFGF-loaded nanoparticles stimulates wound healing in diabetic mice, Acta Biomater. 9 (2013) 7814–7821.
[62] M.D. Cui, Z.H. Pan, L.Q. Pan, Danggui buxue extract-loaded liposomes in thermosensitive gel enhance in vivo dermal wound healing via activation of the VEGF/PI3K/Akt and TGF-beta/smads signaling pathway, Evid Based Complement Alternat Med (2017) 84072492017.
[63] L. Ren, F. Han, L. Xuan, Y. Lv, L. Gong, Y. Yan, Z. Wan, L. Guo, H. Liu, B. Xu, Y. Sun, S. Yang, L. Liu, Clusterin ameliorates endothelial dysfunction in diabetes by suppressing mitochondrial fragmentation, Free Radic. Biol. Med. 145 (2019) 357–373.
[64] A. Alnahdi, A. John, H. Raza, N-acetyl cysteine attenuates oxidative stress and glutathione-dependent redox imbalance caused by high glucose/high palmitic acid treatment in pancreatic Rin-5F cells, PloS One 14 (2019) e0226696.
[65] Y. Liu, X. Tian, Y. Li, D. Liu, M. Liu, X. Zhang, Q. Zhang, C. Yan, Y. Han, Up-regulation of CREG expression by the transcription factor GATA1 inhibits high glucose- and high palmitate-induced apoptosis in human umbilical vein endothelial cells, PloS One 11 (2016) e0154861.
[66] Y. Xie, X. Shi, K. Sheng, G. Han, W. Li, Q. Zhao, B. Jiang, J. Feng, J. Li, Y. Gu, PI3K/Akt signaling transduction pathway, erythropoiesis and glycolysis in hypoxia (Review), Mol. Med. Rep. 19 (2019) 783–791.
[67] Y. Sun, W.Z. Liu, T. Liu, X. Feng, N. Yang, H.F. Zhou, Signaling pathway of MAPK/ERK in cell proliferation, differentiation, migration, senescence and apoptosis, J Recept Sig Transd 35 (2015) 600–604.
[68] J.J. Cui, F.Y. Zhang, Y.S. Wang, J.J. Liu, X. Ming, J.B. Hou, B. Lv, S.H. Fang, B. Yu, Macrophage migration inhibitory factor promotes cardiac stem cell proliferation and endothelial differentiation through the activation of the PI3K/Akt/mTOR and AMPK pathways, Int. J. Mol. Med. 37 (2016) 1299–1309.
[69] G. Hubner, M. Brauchle, H. Smola, M. Madlener, R. Fassler, S. Werner, Differential regulation of pro-inflammatory cytokines during wound healing in normal and glucocorticoid-treated mice, Cytokine 8 (1996) 548–556.
[70] M. Papetti, I.M. Herman, Mechanisms of normal and tumor-derived angiogenesis, Am. J. Physiol. Cell Physiol. 282 (2002) C947–C970.
[71] D.H. Walter, K. Rittig, F.H. Bahlmann, R. Kirchmair, M. Silver, T. Murayama, H. Nishimura, D.W. Losordo, T. Asahara, J.M. Isner, Statin therapy accelerates re-endothelialization: a novel effect involving mobilization and incorporation of bone marrow-derived endothelial progenitor cells, Circulation 105 (2002) 3017–3024.
[72] Y. Duan, S. Yu, P. Xu, X. Wang, X. Feng, Z. Mao, C. Gao, Co-immobilization of CD133 antibodies, vascular endothelial growth factors, and REDV peptide promotes capture, proliferation, and differentiation of endothelial progenitor cells, Acta Biomater. 96 (2019) 137–148.
[73] L. Tarusha, S. Paoletti, A. Travan, E. Marsich, Alginate membranes loaded with hyaluronic acid and silver nanoparticles to foster tissue healing and to control bacterial contamination of non-healing wounds, J. Mater. Sci. Mater. Med. 29 (2018).
[74] A. Scalise, A. Bianchi, C. Tartaglione, E. Bolletta, M. Pierangeli, M. Torresetti, M. Marazzi, G. Di Benedetto, Microenvironment and microbiology of skin wounds: the role of bacterial biofilms and related factors, Semin. Vasc. Surg. 28 (2015) 151–159.
[75] S.M. McCarty, C.A. Cochrane, P.D. Clegg, S.L. Percival, The role of endogenous and exogenous enzymes in chronic wounds: a focus on the implications of aberrant levels of both host and bacterial proteases in wound healing, Wound Repair Regen. 20 (2012) 125–136.
[76] C.R. Kruse, K. Nuutila, C.C. Lee, E. Kiwanuka, M. Singh, E.J. Caterson, E. Eriksson, J.A. Sorensen, The external microenvironment of healing skin wounds, Wound Repair Regen. 23 (2015) 456–464.
[77] K. Ousey, K.F. Cutting, A.A. Rogers, M.G. Rippon, The importance of hydration in wound healing: reinvigorating the clinical perspective, J. Wound Care 25 (2016) 122–130.
[78] K.F. Wlaschin, J. Ninkovic, G.W. Griesgraber, S. Colak Atan, A.J. Young, J.M. Pereira, M.J. Solberg, G. Smith, P.J. Parks, A.K. McNulty, D.L. Langer-Anderson, The impact of first-aid dressing design on healing of porcine partial thickness wounds, Wound Repair Regen. 27 (2019) 622–633.
[79] J.M. Reinke, H. Sorg, Wound repair and regeneration, Eur. Surg. Res. 49 (2012) 35–43.
[80] M.A. Loots, E.N. Lamme, J. Zeegelaar, J.R. Mekkes, J.D. Bos, E. Middelkoop, Differences in cellular infiltrate and extracellular matrix of chronic diabetic and venous ulcers versus acute wounds, J. Invest. Dermatol. 111 (1998) 850–857.
[81] S.A. Eming, T. Krieg, J.M. Davidson, Inflammation in wound repair: molecular and cellular mechanisms, J. Invest. Dermatol. 127 (2007) 514–525.
[82] K.M. Bullard, M.T. Longaker, H.P. Lorenz, Fetal wound healing: current biology, World J. Surg. 27 (2003) 54–61.
[83] M.J. Redd, L. Cooper, W. Wood, B. Stramer, P. Martin, Wound healing and inflammation: embryos reveal the way to perfect repair, Philos. Trans. R. Soc. Lond. B Biol. Sci. 359 (2004) 777–784.
[84] L. Rutter, Obtaining the optimum moist wound healing environment, Br. J. Community Nurs. 22 (2017) S36–S40.
[85] M.G. Rippon, K. Ousey, K.F. Cutting, Wound healing and hyper-hydration: a counterintuitive model, J. Wound Care 25 (2016) 68–75.
[86] X. Wang, J. Chu, C.J. Wen, S.B. Fu, Y.L. Qian, Y. Wo, C. Wang, D.R. Wang, Functional characterization of TRAP1-like protein involved in modulating fibrotic processes mediated by TGF-beta/Smad signaling in hypertrophic scar fibroblasts, Exp. Cell Res. 332 (2015) 202–211.
[87] C. Huang, S. Akaishi, R. Ogawa, Mechanosignaling pathways in cutaneous scarring, Arch. Dermatol. Res. 304 (2012) 589–597.
[88] W. Shen, Y. Wang, D. Wang, H. Zhou, H. Zhang, L. Li, miR-145-5p attenuates hypertrophic scar via reducing Smad2/Smad3 expression, Biochem. Biophys. Res. Commun. 521 (2020) 1042–1048.
[89] E.B. Katzel, M. Wolenski, A.E. Loiselle, P. Basile, L.M. Flick, H.N. Langstein, M.J. Hilton, H.A. Awad, W.C. Hammert, R.J. O'Keefe, Impact of Smad3 loss of function on scarring and adhesion formation during tendon healing, J. Orthop. Res. 29 (2011) 684–693.
[90] I. Kolosova, D. Nethery, J.A. Kern, Role of Smad2/3 and p38 MAP kinase in TGF-beta1-induced epithelial-mesenchymal transition of pulmonary epithelial cells, J. Cell. Physiol. 226 (2011) 1248–1254.